Proceedings of the ASME 2023
42nd International Conference on Ocean, Offshore Arctic Engineering
OMAE2023
June 11–16, 2023, Melbourne, Australia

OMAE2023-102570

A DECENTRALIZED DROOP-BASED POWER MANAGEMENT SYSTEM FOR SHIP POWER SYSTEMS USING HYBRID DYNAMICAL SYSTEMS FRAMEWORK

Namireddy Praveen Reddy[1,†,*], Roger Skjetne[1], Dimitrios Papageorgiou[2]

[1]Norwegian University of Science and Technology, Trondheim, Norway
[2]Technical University of Denmark, Copenhagen, Denmark

ABSTRACT

In maritime transport, inspired by the automobile sector, autonomy is gaining traction in parallel with decarbonization. One of the numerous challenges in realizing fully autonomous operation in shipping is to design a resilient and fault-tolerant power system that preserves the survivability of ships during worst-case failures in unpredictable maritime weather conditions. In newly built ships, power systems are designed with a high number of sensors and communication equipment to enable remote control and condition monitoring in real time. In such power systems, the traditional concept of a centralized power management system (PMS) is not reliable during communication failures and cyberattacks. To address this issue a decentralized fault-tolerant droop-based PMS that does not rely on communication between energy sources is proposed. The droop curves are further designed for the derating operation of energy sources and energy storage devices. A ship power system exposed to faults represents a hybrid system that consists of interaction between continuous and discrete states. Hybrid dynamical systems theory is used to model the DC power system and implement the proposed PMS. The normal operation of energy sources, energy storage devices, and shiploads are modeled as continuous dynamics. The faults such as derating operation and disconnection of energy sources, energy storage devices, and shiploads are modeled as discrete events. The results demonstrate that the proposed PMS can keep the system parameters such as DC bus voltage within the limits permissible by class rules during the loss of power generation.

Keywords: Droop control, Fault-tolerant power management system, Hybrid dynamical systems, Ship power systems

1. INTRODUCTION

Autonomous ships with all-electric power and propulsion systems have generated considerable research and development interest in recent years inspired by the automobile sector [1]. The design of onboard power systems for autonomous ships brings in numerous challenges. The autonomous ship's power system is fully digitalized to enable remote condition monitoring and control. Consequently, there will be more sensors and communication systems compared to conventional counterparts. To preserve the survivability of ships during worst-case failures in unpredictable weather conditions, it is important to design a resilient power system that is fault-tolerant with respect to faults in physical components, sensors, actuators, and communication systems. Traditionally, shipboard power systems have a centralized controller, i.e., a power management system (PMS) that commands local controllers. The PMS can be designed from simple rule-based algorithms to more advanced intelligent algorithms based on artificial intelligence [2]. There is extensive literature on PMS for different modes of transportation solutions such as land-based, waterborne, and airborne. The existing literature covers multiple objectives ranging from fuel consumption optimization to prolonging components' life to fault-tolerance capabilities with different methods to meet these objectives [3]. However, when there is a communication failure, the centralized controller may become inoperable with a risk to survivability, which is essential in waterborne and airborne transportation [4]. PMS based on droop control inherently addresses the issue of communication delays and communication failures as it does not depend on communication between different components [5].

A decentralized control approach based on conventional and improved droop control is presented for autonomous AC microgrids in [6]. The adaptive droop was proposed to control the source current during short-circuit faults by calculating a virtual impedance to control the converter output reference voltage and, thus, increasing the fault clearance time by 60 microseconds [7]. The conventional droop control has several limitations, such as current sharing inaccuracy, which may affect the system stability in case of line impedance mismatch [8]. To overcome these issues, a distributed control scheme was proposed that modi-

[†]Joint first authors
[*]Corresponding author: namireddy.p.reddy@ntnu.no
Documentation for `asmeconf.cls`: Version 1.32, November 6, 2023.

fied the effective droop gain to achieve good voltage regulation and accurate load sharing [9]. An improved distributed secondary control scheme was proposed that can remove the DC voltage deviation and improve the current sharing accuracy by using voltage-shifting and slope-adjusting approaches simultaneously, aiming at overcoming the drawbacks of conventional droop control method [10]. An adaptive distributed secondary droop controller, which varied the slope of the output voltage–current characteristics and shifts the output voltage across each load to a reference bus voltage, was proposed in [11]. SOC-dependent adaptive droop control was used to improve the battery life by making the battery at higher SOC have slow charging and fast discharging [12]. Faults such as disconnection and derating of energy sources and loads are not considered while designing PMS based on droop control in the existing literature. Shipboard hybrid electric power systems during faults may be considered to have both *continuous-time* and *discrete-time* dynamics. To analyze such systems, the hybrid dynamical systems approach combines *continuous-time* and *discrete-time* dynamics and offers a systemic approach for stability analysis [13]. However, this is not extensively applied on ship power systems except in a few works such as [14]–[16]. To fill the research gap, a fault-tolerant droop-based PMS is proposed in this paper, designed in the hybrid dynamical systems framework. The main contributions of this paper are 1) modeling of the shipboard hybrid power system in the hybrid dynamical systems framework, 2) proposing a fault-tolerant PMS based on droop control, 3) designing droop curves to enable the derating operation of power generation sources, and 4) investigate the effect of loss of power generating units on the voltage (V) to active power (P) droop-based load-sharing, with the implementation of a fault-tolerant V-P droop load sharing.

2. SHIP POWER SYSTEM MODEL

A single-line diagram of a typical shipboard DC hybrid power system is shown in Figure. 1. During normal operation,

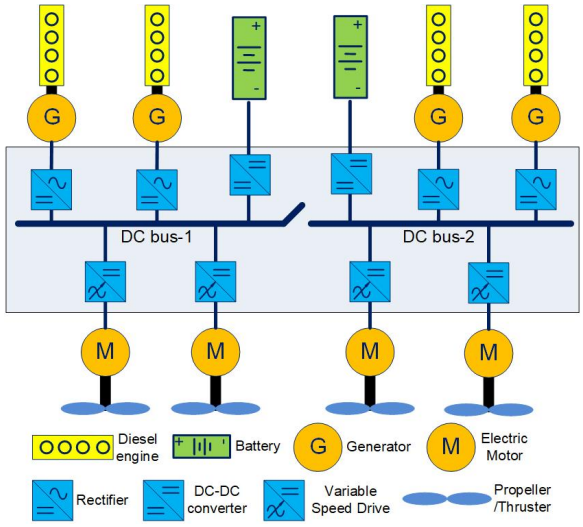

FIGURE 1: SLD OF A TYPICAL HYBRID POWER SYSTEM

the DC bus is sectionalized into two buses, namely DC bus-1 and DC bus-2. In this work, the case study is one of the identical sectionalized buses. The ship's power system can be represented as a hybrid dynamical system due to switching dynamics under faults [13].

2.1 Continuous system dynamics

The continuous dynamics of various components in a diesel engine generator set can be represented in the model. The diesel engine is represented by a time delay, the shaft is represented by the swing equation, the generator is represented in dq framework, and the rectifier is represented either by either dq framework or an average model. However, for control design, simplified models are used depending on the intended use. In this work, a first-order lowpass filter is used to represent the diesel engine generator sets,

$$\dot{P}_g = -\frac{K}{\tau}(-P_{g,r} + P_g) \tag{1}$$

where, $\dot{P}_g$ is the time derivative of genset power, $P_{g,r}$ is genset power reference, P_g is the power measured, K is a proportionality constant, and τ is a time constant. Typically, in a hybrid power system, one of the gensets or batteries is in voltage control mode. In this case study, the DC bus voltage is controlled by Genset-2 and there is an additional additive input (u) in its power dynamics ($\dot{P}_{g_2}$) which is generated through a PI controller with DC bus voltage error (e_v) and power-generated error (e_p) as inputs, that is,

$$\dot{P}_{g_2} = -\frac{K}{\tau}(-P_{g_2,r} + P_{g_2}) + u \tag{2}$$

$$u = K_{p_v} \times e_v + K_{i_v} \int_0^t e_v dt + K_{p_p} \times e_p + K_{i_p} \int_0^t e_p dt$$
$$e_v = V_{dc,r} - V_{dc}$$
$$e_p = P_{g_2,r} - P_{g_2},$$

where K_{p_v} & K_{p_p} are proportionality gains and K_{i_v} & K_{i_p} are integral gains of PI controller. K_{p_p} & K_{i_p} are set to 0 in this work. The battery's state of charge (SOC) is represented by the coulomb counting method,

$$S = S_0 - \frac{1}{Q_r}\int_0^t P_b dt, \tag{3}$$

$$\dot{S} = -\frac{P_b}{Q_r} \tag{4}$$

where S is the SOC of the battery bank, S_0 is the initial value, Q_r is the rated energy capacity of the battery bank, and P_b is the power output of the battery, given by $P_b = P_L - P_g$; with a positive sign during discharging and negative sign during charging. The dynamics of the DC bus voltage (V_{dc}) are represented using the following differential equation,

$$\dot{V}_{dc} = \frac{1}{C_{dc}V_{dc}}\left(\underbrace{\sum_{i=1}^{m} P_{g,i} + \sum_{i=1}^{n} P_{b,i}}_{P_{supply}} - \underbrace{\sum_{i=1}^{p} P_{L,i}}_{P_{demand}}\right), \tag{5}$$

where C_{dc} is the capacitance of the DC-link capacitor, m is the number of diesel engines, n is the number of battery banks, and p is the number of shiploads. It is assumed that the power electronic converters that interface the gensets and battery banks with the DC bus are lossless and work perfectly according to the references given by the V-P droop-based PMS.

2.2 Discrete-event system (DES) dynamics

The discrete system dynamics are represented by events such as the disconnection and derating of power system components including gensets, battery banks, and shiploads [17]. Power system components are disconnected when faults such as short circuits occur, which does not allow continuity of operation. The derating operation of a genset may be necessary due to operating conditions such as high temperature, air quality, and fuel quality. Inefficiencies in a cooling system can result in higher engine fluid temperatures. For example, when the diesel engine is operated at high altitudes or high temperatures, the oxygen percentage in the air is reduced resulting in compromised air quality. The fuel volumetric energy density and fuel temperature affect the engine output power. The aging of batteries depends on many factors such as charge-discharge cycles, depth of discharge (DOD), and C-rate [18] [19]. Batteries can be operated at reduced capacity to prolong life or due to high operating temperatures. Non-essential shiploads can be disconnected either due to faults or load-shedding. Load-shedding or fast load reduction (FLR) is necessary to keep the DC bus voltage within the operational limits when there is less available power supply than demand. However, essential loads such as propulsion loads should only be reduced when load reduction is necessary.

An indicator $q \in [0, 1]$ is used to represent the discrete system dynamics. $q = 1$ indicates normal operation, $q = 0$ indicates the disconnection due to fault, and other values indicate the derating operation based on the derating factor ($DF = \frac{\text{Available capacity}}{\text{Rated capacity}}$), that is,

$$q = \begin{cases} 1 & \text{normal operation} \\ DF \in (0, 1) & \text{derated operation} \\ 0 & \text{disconnection.} \end{cases} \tag{6}$$

3. POWER MANAGEMENT SYSTEM

The power management system (PMS) is designed based on the V-P droop-based loadsharing. The droop equations for the given hybrid power system are

$$\begin{bmatrix} 1 & K_{g,1} & 0 & 0 \\ 1 & 0 & K_{g,2} & 0 \\ 1 & 0 & 0 & K_{b,1} \\ 0 & 1 & 1 & 1 \end{bmatrix} \begin{bmatrix} V_{dc,r} \\ P_{g,1,r} \\ P_{g,2,r} \\ P_{b,1,r} \end{bmatrix} = \begin{bmatrix} V_{nl,g,1} \\ V_{nl,g,2} \\ V_{nl,b,1} \\ P_L \end{bmatrix},$$

where $V_{dc,r}$ is the DC bus voltage reference, $P_{g,i,r}$ and $P_{b,i,r}$ are power references generated by PMS for the diesel engines and battery bank, respectively, $V_{nl,g,i}$ and $V_{nl,b,i}$ are the no-load voltages of diesel engines and battery bank, respectively, and P_L is the load power required. $K_{g,i}$ and $K_{b,i}$ are the droop gains of diesel engines and battery banks, respectively, computed by

$$K_{g,i} = \frac{V_{nl,g,i} - V_{P_{max},g,i}}{q_{g,i} P_{max,g,i}}, \tag{7}$$

where $P_{max,g,i}$ is the maximum power, and $V_{P_{max},g,i}$ is the voltage at maximum power of the i^{th} genset. If the DC bus voltage regulation is assumed 10 %, then

$$V_{nl,g,i} = 1.05 V_{dc,rated}$$
$$V_{P_{max},g,i} = 0.95 V_{dc,rated}.$$

For the battery, $K_{b,i}$ is computed as

$$K_{b,i} = \begin{cases} \left.\begin{array}{l} \frac{V_{P_{ch,max}} - V_{P_{dch,max}}}{q_{b,i}(P_{ch,max} - P_{dch,max})} \\ V_{P_{ch,max}} = 1.05 V_{dc,rated} \\ V_{P_{dch,max}} = 0.95 V_{dc,rated} \end{array}\right\} SOC_{min} < SOC < SOC_{max} \\ \left.\begin{array}{l} \frac{V_{nl,b,i} - V_{P_{ch,max}}}{q_{b,i} P_{ch,max}} \\ V_{nl,b,i} = 0.95 V_{dc,rated} \\ V_{P_{ch,max}} = 1.05 V_{dc,rated} \end{array}\right\} SOC \le SOC_{min} \\ \left.\begin{array}{l} \frac{V_{nl,b,i} - V_{P_{dch,max}}}{q_{b,i} P_{dch,max}} \\ V_{nl,b,i} = 1.05 V_{dc,rated} \\ V_{P_{dch,max}} = 0.95 V_{dc,rated} \end{array}\right\} SOC \ge SOC_{max}, \end{cases}$$

where $P_{ch,max}$ is the maximum charging power and $P_{dch,max}$ is the maximum discharging power. $V_{P_{ch,max}}$ and $V_{P_{dch,max}}$ are the voltages at maximum charging power and maximum discharging power, respectively. The droop curves during normal operation and derating operation are shown in Figure. 2 and Figure. 3, respectively, whereas the flowchart for the droop-based PMS is

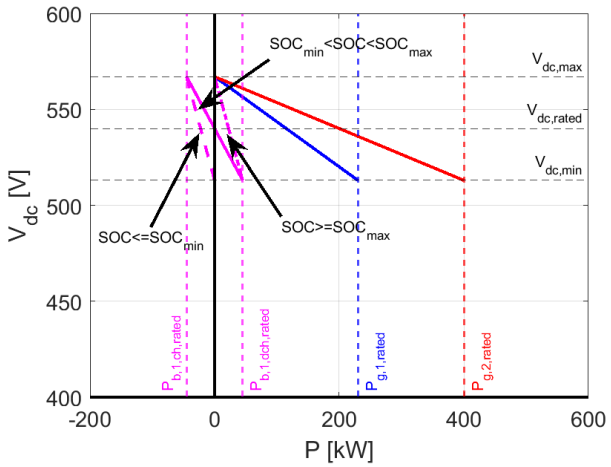

FIGURE 2: DROOP CURVES OF GENSET 1 (BLUE), GENSET 2 (RED), AND BATTERY BANK 1 (MAGENTA).

shown in Figure. 4. To make the droop controller fault-tolerant, the algorithm shown in flow chart is implemented. When there is a fault in one of the components, the faulty component is isolated

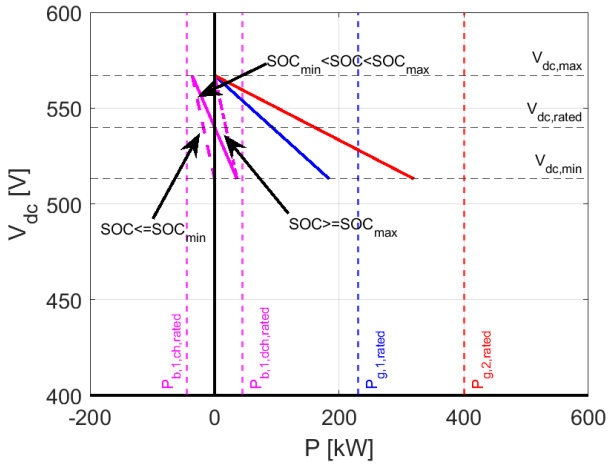

FIGURE 3: DROOP CURVES OF GENSET 1 (BLUE), GENSET 2 (RED), AND BATTERY BANK 1 (MAGENTA) DURING DERATED OPERATION WITH DERATING FACTOR OF 0.8 PU.

and the load power is redistributed among the healthy sources. If, after a fault, the total power supply capacity is lower than the load demand, then the additional loads are either reduced or disconnected.

4. HYBRID DYNAMICAL SYSTEMS FRAMEWORK

A typical hybrid dynamical system consists of system states $x \in \mathbb{R}^n$, which have continuous dynamics during flows and discrete dynamics during jumps. A hybrid dynamical system is represented mathematically by,

$$\mathcal{H}: \begin{cases} x \in C & \overbrace{\dot{x} \in F(x)}^{\text{differential inclusion}} \quad \textbf{or} \quad \overbrace{\dot{x} = f(x)}^{\text{differential equation}} \\ x \in D & \underbrace{x^+ \in G(x)}_{\text{difference inclusion}} \quad \textbf{or} \quad \underbrace{x^+ = g(x)}_{\text{difference equation}} \end{cases}, \tag{8}$$

where $C \subset \mathbb{R}^n$ is a flow set where the system state evolves according to either the differential inclusion $\dot{x} \in F(x)$ or the differential equation $\dot{x} = f(x)$. $D \subset \mathbb{R}^n$ is a jump set where the system state evolves according to either the difference inclusion $x^+ \in G(x)$ or the difference equation $x^+ \in g(x)$. In this paper, the flow map is a differential inclusion ($F(x)$), and the jump map is a difference inclusion ($G(x)$). In this case study, the system state is $x := [P_{g,i}\, V_{dc}\, \zeta_v\, S_{b,i}\, q_{g,i}\, q_{b,i}\, q_{L,i}\, t]$, where $\zeta_v = \int_0^t e_v dt$ and t is simulation time. The flow map ($F(x)$) is derived from the differential inclusions,

$$F(x) := \begin{bmatrix} -\frac{K}{\tau}(-P_{g,i,r} + P_{g,i}) \\ \frac{1}{C_{dc} V_{dc}} \left(\sum_{i=1}^{m} P_{g,i} + \sum_{i=1}^{n} P_{b,i} - \sum_{i=1}^{p} P_{L,i} \right) \\ V_{dc,r} - V_{dc} \\ -\frac{P_b}{E_{r,b}} \\ 0 \\ 0 \\ 0 \\ 1 \end{bmatrix}, \tag{9}$$

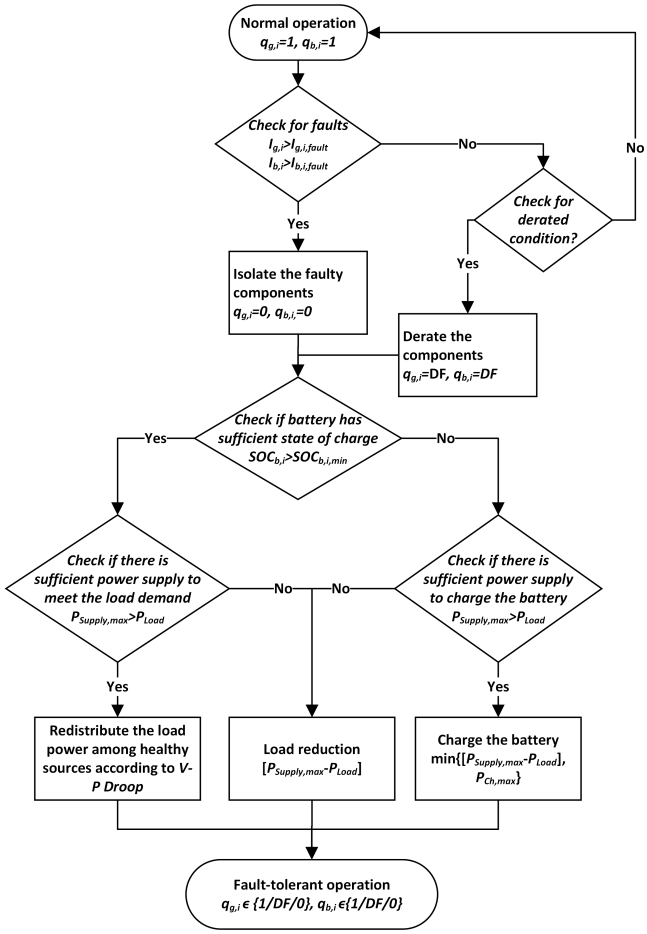

FIGURE 4: FLOWCHART OF DROOP-BASED PMS

and the jump map ($G(x)$) is derived from the difference inclusions,

$$G(x) := \begin{bmatrix} P_{g,i} \\ V_{dc} \\ \zeta_v \\ S_{b,i} \\ q_{g,i} \in [0,\ 1] \\ q_{b,i} \in [0,\ 1] \\ q_{L,i} \in [0,\ 1] \\ t \end{bmatrix}. \tag{10}$$

The flow set (C) is the union of three subsets C_1, C_2, and C_3 representing the flow sets for the connected gensets, battery banks, and shiploads, respectively. In reality, the flow sets are defined using physical parameters such as current ($I_{g/b/L}$) and operational temperature ($T_{g/b/L}$) that are within the specified limits. Currents in the connected gensets, battery banks, and shiploads can be computed by dividing the respective powers by DC bus voltage. However, in this work, the simulation time is used instead of temperature, due to the unavailability of temperature as a system state in the simplified system model.

$$C = C_1 \cup C_2 \cup C_3$$

$$C_1 = \begin{cases} [0,400]^2 \times [513,567] \times [-27,27] \\ \times [0,100] \times [0,1] \times [0,1] \times [0,1] \times \\ [0,200]: \begin{cases} q_{g,i} \neq 0 \ \& \ I_{g,i} < I_{g,i,f} \ \& \ t \neq t_{g,i,df} \end{cases} \end{cases}$$

$$C_2 = \begin{cases} [0,400]^2 \times [513,567] \times [-27,27] \\ \times [0,100] \times [0,1] \times [0,1] \times [0,1] \times \\ [0,200]: \begin{cases} q_b \neq 0 \ \& \ I_b < I_{b,f} \ \& \ t \neq t_{b,df} \end{cases} \end{cases}$$

$$C_3 = \begin{cases} [0,400]^2 \times [513,567] \times [-27,27] \\ \times [0,100] \times [0,1] \times [0,1] \times [0,1] \times \\ [0,200]: \begin{cases} q_L \neq 0 \ \& \ I_L < I_{L,f} \ \& \ P_{supply} \geq P_{demand} \end{cases} \end{cases},$$

where $I_{g,i} = \frac{P_{g,i}}{V_{dc}}$, $I_b = \frac{P_b}{V_{dc}}$, and $I_L = \frac{P_L}{V_{dc}}$. $I_{g,f}$, $I_{b,f}$, and $I_{L,f}$ are the thresholds to determine the faulty operation of gensets, battery bank, and loads, respectively. $t_{g,i,df}$ and $t_{b,df}$ are simulation times at which derating is implemented in connected gensets and battery banks, respectively.

The jump set (D) is the union of three subsets D_1, D_2, and D_3 that represent the jump sets for the connected gensets, battery banks, and shiploads, respectively.

$$D = D_1 \cup D_2 \cup D_3$$

$$D_1 = \begin{cases} [0,400]^2 \times [513,567] \times [-27,27] \\ \times [0,100] \times [0,1] \times [0,1] \times [0,1] \times \\ [0,200]: \begin{cases} disconnection: q_{g,i} \in (0,1] \ \& \ I_{g,i} \geq I_{g,i,f} \\ derating: q_{g,i} = 1 \ \& \ t = t_{g,i,df} \end{cases} \end{cases}$$

$$D_2 = \begin{cases} [0,400]^2 \times [513,567] \times [-27,27] \\ \times [0,100] \times [0,1] \times [0,1] \times [0,1] \times \\ [0,200]: \begin{cases} disconnection: q_b \in (0,1] \ \& \ I_b \geq I_{b,f} \\ derating: q_b = 1 \ \& \ t = t_{b,df} \end{cases} \end{cases}$$

$$D_3 = \begin{cases} [0,400]^2 \times [513,567] \times [-27,27] \\ \times [0,100] \times [0,1] \times [0,1] \times [0,1] \times \\ [0,200]: \begin{cases} disconnection: q_L \in (0,1] \ \& \ I_L \geq I_{L,f} \\ derating: q_L = 1 \ \& \ P_{supply} < P_{demand} \end{cases} \end{cases},$$

5. RESULTS

In this section, the proposed PMS is validated through the simulation of two possible events i.e., disconnection and derating operation of one of the gensets in the considered shipboard hybrid power system. Both the gensets are assumed to be identical which is usually the case in ships. These switching events are created based on the simulation time (at 50 seconds) due to the simplified control plant model; where it is not possible to simulate the physical conditions required for the detection of switching events.

Figure. 5 and Figure. 6 show the DC bus voltage profile and the power profiles including load power, genset powers, and battery power for two conditions; 1) derating and disconnection of one genset at fixed load power of 400 kW and varying derating factor, and 2) derating of one genset at varying load power and fixed derating factor. It can be observed that the load power can not be more than 400 kW to ensure the DC bus voltage remains within the permissible limits when one of the gensets is disconnected ($q_{g,1} = 0$). However, the limit on maximum load power can be higher when the derating of the genset is considered. For example, as shown in Figure. 5 and Figure. 6, a maximum limit of 700 kW is allowed when one of the gensets is operated at 75 % of the capacity (derating factor = 0.75). However, the maximum limit on the load power is reduced to 600 kW when the derating factor is reduced to 0.50. Therefore, the maximum load power allowed can be increased for a higher derating factor.

6. CONCLUSION

In this paper, a PMS control function for a hybrid power system is designed and implemented based on droop control in a hybrid dynamical systems framework. Disconnection and derating of gensets are modeled as faults, i.e, discrete events. The analysis is performed to derive the conditions required for DC bus voltage stability. The simulation results show that considering the derating operation in droop-based PMS will result in the increase of maximum load power compared with the disconnection of genset, that is, for some operating conditions which do not require disconnection of a genset. Future work is validation of the proposal using a high-fidelity model of the ship power system considered. Moreover, fault detection and diagnosis can be implemented and integrated with the proposed PMS.

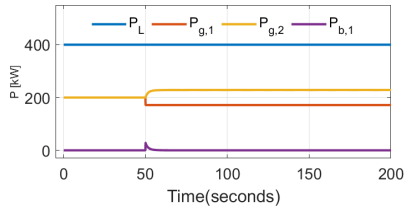

(a) Power profiles (P_L = 400, $q_{g,1}$ = 0.75)

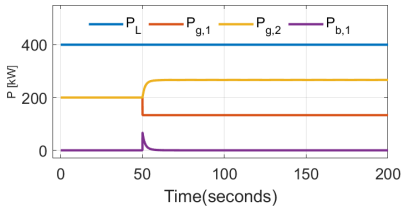

(b) Power profiles (P_L = 400, $q_{g,1}$ = 0.50)

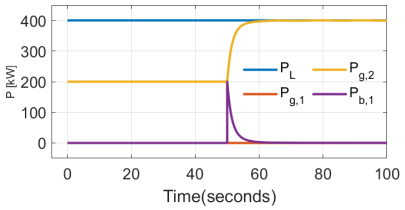

(c) Power profiles (P_L = 400, $q_{g,1}$ = 0)

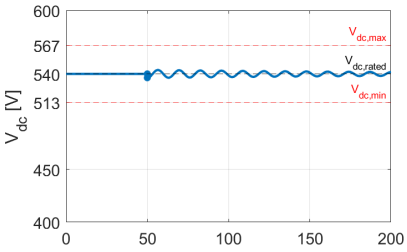

(d) V_{dc} profile (P_L = 400, $q_{g,1}$ = 0.75)

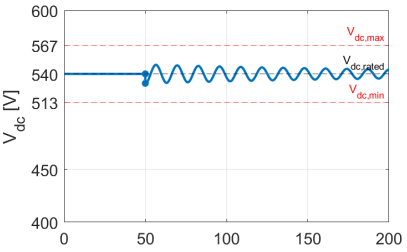

(e) V_{dc} profile (P_L = 400, $q_{g,1}$ = 0.50)

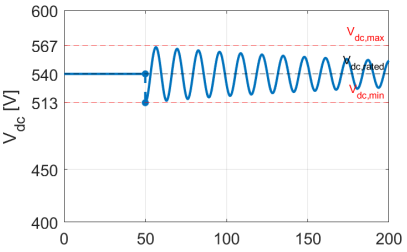

(f) V_{dc} profile (P_L = 400, $q_{g,1}$ = 0)

FIGURE 5: COMPARISON OF POWER & VOLTAGE FOR DIFFERENT DERATING FACTORS (DISCONNECTION & DERATING) AND FIXED LOAD POWER

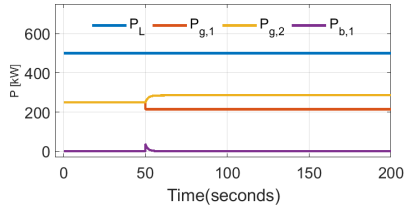

(a) Power profiles (P_L = 500, $q_{g,1}$ = 0.75)

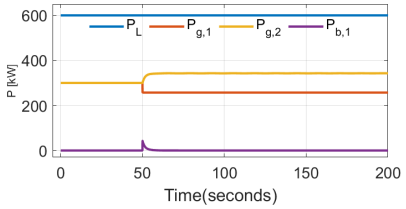

(b) Power profiles (P_L = 600, $q_{g,1}$ = 0.75)

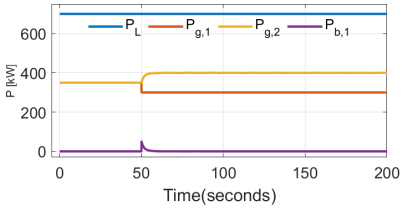

(c) Power profiles (P_L = 700, $q_{g,1}$ = 0.75)

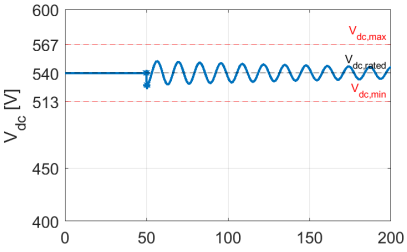

(d) V_{dc} profile (P_L = 500, $q_{g,1}$ = 0.75)

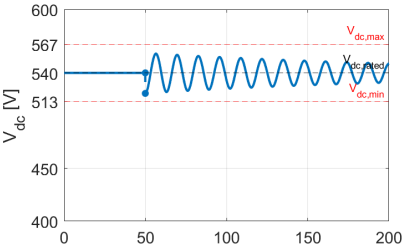

(e) V_{dc} profile (P_L = 600, $q_{g,1}$ = 0.75)

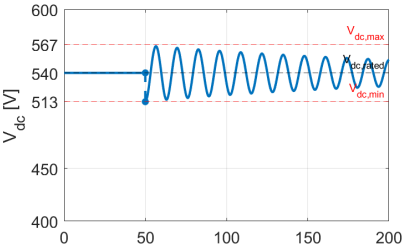

(f) V_{dc} profile (P_L = 700, $q_{g,1}$ = 0.75)

FIGURE 6: COMPARISON OF POWER AND VOLTAGE FOR DIFFERENT LOAD POWERS AND FIXED DE-RATING FACTOR

REFERENCES

[1] N. P. Reddy, M. K. Zadeh, C. A. Thieme, *et al.*, "Zero-Emission Autonomous Ferries for Urban Water Transport: Cheaper, Cleaner Alternative to Bridges and Manned Vessels," *IEEE Electrification Magazine*, vol. 7, no. 4, pp. 32–45, Dec. 2019.

[2] P. Xie, J. M. Guerrero, S. Tan, *et al.*, "Optimization-Based Power and Energy Management System in Shipboard Microgrid: A Review," *IEEE Systems Journal*, pp. 1–13, 2021.

[3] N. Sulaiman, M. A. Hannan, A. Mohamed, P. J. Ker, E. H. Majlan, and W. R. Wan Daud, "Optimization of energy management system for fuel-cell hybrid electric vehicles: Issues and recommendations," *Applied Energy*, vol. 228, pp. 2061–2079, Oct. 2018.

[4] M. D. A. Al-Falahi, T. Tarasiuk, S. G. Jayasinghe, Z. Jin, H. Enshaei, and J. M. Guerrero, "AC Ship Microgrids: Control and Power Management Optimization," en, *Energies*, vol. 11, no. 6, p. 1458, 2018.

[5] M. Babaei, J. Shi, and S. Abdelwahed, "A Survey on Fault Detection, Isolation, and Reconfiguration Methods in Electric Ship Power Systems," *IEEE Access*, vol. 6, pp. 9430–9441, 2018.

[6] L. S. De Araujo, A. M. D. S. Alonso, and D. I. Brandao, "Decentralized Control of Voltage- and Current-Controlled Converters Based on AC Bus Signaling for Autonomous Microgrids," *IEEE Access*, vol. 8, pp. 202 075–202 089, 2020.

[7] S. Augustine, M. J. Reno, S. M. Brahma, and O. Lavrova, "Fault Current Control and Protection in a Standalone DC Microgrid Using Adaptive Droop and Current Derivative," *IEEE Journal of Emerging and Selected Topics in Power Electronics*, vol. 9, no. 3, pp. 2529–2539, Jun. 2021.

[8] S. Adhikari, Y. Tang, and P. Wang, "Secondary control for DC microgrids: A review," in *2016 Asian Conference on Energy, Power and Transportation Electrification (ACEPT)*, Oct. 2016, pp. 1–6.

[9] A. Tah and D. Das, "An Enhanced Droop Control Method for Accurate Load Sharing and Voltage Improvement of Isolated and Interconnected DC Microgrids," *IEEE Transactions on Sustainable Energy*, vol. 7, no. 3, pp. 1194–1204, Jul. 2016.

[10] P. Wang, X. Lu, X. Yang, W. Wang, and D. Xu, "An Improved Distributed Secondary Control Method for DC Microgrids With Enhanced Dynamic Current Sharing Performance," *IEEE Transactions on Power Electronics*, vol. 31, no. 9, pp. 6658–6673, Sep. 2016.

[11] R. Kumar and M. K. Pathak, "Distributed droop control of dc microgrid for improved voltage regulation and current sharing," en, *IET Renewable Power Generation*, vol. 14, no. 13, pp. 2499–2506, 2020.

[12] L. Xu, B. Wei, Y. Yu, J. M. Guerrero, and J. Vasquez, "Coordinated Control of Diesel Generators and Batteries in DC Hybrid Electric Shipboard Power System," en, *Energies*, vol. 14, no. 19, p. 6246, Jan. 2021.

[13] R. Goebel, R. G. Sanfelice, and A. R. Teel, *Hybrid Dynamical Systems: Modeling, Stability, and Robustness*, en. Mar. 2012.

[14] L. Thorat and R. Skjetne, "Load-dependent start-stop of gensets modeled as a hybrid dynamical system," en, 20th IFAC World Congress, vol. 50, no. 1, pp. 9321–9328, Jul. 2017.

[15] M. R. Miyazaki, A. J. Sørensen, and B. J. Vartdal, "Hybrid marine power plants model validation with strategic loading," en, 10th IFAC CAMS, vol. 49, no. 23, pp. 400–407, Jan. 2016.

[16] D. Park, M. K. Zadeh, and R. Skjetne, "DC-DC Converter Control for Peak-Shaving in Shipboard DC Power System via Hybrid Control," in *2020 15th IEEE Conference on Industrial Electronics and Applications (ICIEA)*, ISSN: 2158-2297, Nov. 2020, pp. 681–686.

[17] C. G. Cassandras and S. Lafortune, "Introduction to Queueing Theory," en, in *Introduction to Discrete Event Systems*, C. G. Cassandras and S. Lafortune, Eds., Cham: Springer International Publishing, 2021, pp. 465–533.

[18] B. Xu, A. Oudalov, A. Ulbig, G. Andersson, and D. S. Kirschen, "Modeling of Lithium-Ion Battery Degradation for Cell Life Assessment," *IEEE Transactions on Smart Grid*, vol. 9, no. 2, pp. 1131–1140, Mar. 2018.

[19] L. Lu, X. Han, J. Li, J. Hua, and M. Ouyang, "A review on the key issues for lithium-ion battery management in electric vehicles," en, *Journal of Power Sources*, vol. 226, pp. 272–288, Mar. 2013.